

Chaos in a well : Effects of competing length scales

R. Sankaranarayanan*, A. Lakshminarayan† and V. B. Sheorey‡

*Physical Research Laboratory,
Navrangpura, Ahmedabad 380 009, India.*

Abstract

A discontinuous generalization of the standard map, which arises naturally as the dynamics of a periodically kicked particle in a one dimensional infinite square well potential, is examined. Existence of competing length scales, namely the width of the well and the wavelength of the external field, introduce novel dynamical behaviour. Deterministic chaos induced diffusion is observed for weak field strengths as the length scales do not match. This is related to an abrupt breakdown of rotationally invariant curves and in particular KAM tori. An approximate stability theory is derived wherein the usual standard map is a point of “bifurcation”.

PACS number(s) : 05.45Ac, 45.05.+x, 47.52.+j

Keywords : Chaos

I. INTRODUCTION

The construction and study of area preserving mappings has led to a deeper understanding of apparently complex dynamics, especially of Hamiltonian chaos. The maps range from abstract models [1] such as the cat maps and the baker map to more generic ones. One of the most well studied of such generic mappings is the standard map [2], which has also been investigated extensively in its quantum version [3]. The classical map on the cylinder displays a range of dynamical behaviours, and when completely chaotic, diffusive random walks in momentum take place. Recent experiments using trapped ultra-cold sodium atoms in pulsed laser fields have probed this model, as a kicked rotator, and verified the central phenomenon of quantum localization of momentum diffusion [4].

In this Letter we study the classical dynamics of a simple generalization of the standard map that naturally arises from the dynamics of a particle trapped in a one dimensional infinitely deep well. The virtue of this generalization is that on the introduction of a competing

*sankar@prl.ernet.in

†arul@prl.ernet.in

‡sheorey@prl.ernet.in

length scale novel dynamical behaviour manifests, leading to large scale diffusive processes even for small external field strengths. This places the standard map within a family of generally discontinuous area preserving mappings; the points where there is continuity corresponding to the usual standard map.

We study the novel dynamical changes by simple methods exploiting separation of time scales in non-autonomous equations. The failure of the Poincaré-Birkhoff theorem leads to the formation of entirely stable islands and cantori or entirely unstable and chaotic orbits. It is also to be pointed out that this can be one of the methods of controlling or enhancing chaos.

The classical motion of a particle in an infinite square well potential in the presence of a uniform monochromatic external field has been studied previously [5]. In this case diffusion was observed over a limited range of energies and there is no issue of competing length scales. Also, no analytic form of the stroboscopic mapping is derivable. We have considered below a space variation of the external field that is also pulsed in time, the pulsing leading to analytically derivable mappings. More recently a special case of this system was studied [6] and quantized, where (in the chaotic regime) an important effect was found, namely delocalization of eigenstates as opposed to the well known exponentially localized states of the kicked rotator. Our independent and parallel studies are a generalization and in this Letter we present the classical aspects as we feel that these deserve a more complete understanding.

Recent advances in semiconductor physics, makes it possible to construct wells on atomic scales. Also, developments in investigating the quantum nature of electrons in a finite quantum well have been achieved, using tunnel-current spectroscopy, when the corresponding classical system shows chaotic behaviour [7] (see references therein). We hope that the study of novel dynamical behaviours in simple models, as the generalization of the standard map, will reflect on some aspects of such experimentally realizable systems.

II. KICKED PARTICLE IN A WELL

We consider a particle of mass m , trapped in an one dimensional infinite square well potential $V_{sq}(x)$ of width $2a$. There is an external field $V(x)$ that is periodically pulsed with period T . The Hamiltonian is

$$H = \frac{p^2}{2m} + V_{sq}(x) + V(x) \sum_{j=-\infty}^{\infty} \delta\left(j - \frac{t}{T}\right) \quad (1)$$

where x, p are the position and momentum of the particle respectively. We consider below $V(x) = \epsilon \cos(2\pi x/\lambda)$. Here ϵ and λ are the amplitude and wavelength of the external field respectively. The effect of the pulsed field in H is the same as that of an infinite number of travelling waves with identical amplitudes and frequencies which are multiples of $2\pi/T$ (the pulse frequency).

The stroboscopic map, relating the dynamical variables immediately after successive kicks, can be derived in a standard manner and results in the following dimensionless form:

$$\begin{aligned} X_{n+1} &= (-1)^{M_n}(X_n + P_n) + (-1)^{M_n+1} \text{Sgn}(P_n) M_n \\ P_{n+1} &= (-1)^{M_n} P_n + (K/2\pi) \sin(2\pi R X_{n+1}). \end{aligned} \quad (2)$$

where $M_n = \left[\text{Sgn}(P_n)(X_n + P_n) + \frac{1}{2} \right]$, is the number of bounces of the particle at the walls during the interval between the n th kick and the $(n+1)$ th kick. Here $\text{Sgn}(\cdot)$ and $[\cdot]$ stand for sign and integer part of the argument respectively. The dimensionless quantities are defined as

$$X_n = \frac{x_n}{2a}, \quad P_n = \frac{p_n T}{2am}, \quad K = \frac{2\epsilon\pi^2 T^2}{am\lambda}, \quad R = \frac{2a}{\lambda}. \quad (3)$$

while the dynamical variables x_n, p_n are the position and momentum of the particle just after the n th kick. Although $\text{Sgn}(P_n)$ is discontinuous and undefined for $P_n = 0$, one can see easily from the map that either of the values (± 1) can be taken for $\text{Sgn}(P_n)$ as this does not alter the dynamics. We refer to the mapping (2) as the *well map*. Note that K and R are the only two effective parameters of the well map. Here K is related to the strength of the external field; R is the ratio of the width of the well to the wavelength of the external field. We do not impose any constraints on R , for example those while considering standing waves in a cavity, but allow it all values. Evidently, $|X_n| \leq 1/2$ or $|x_n| \leq a$ as the particle motion is confined between two rigid walls.

We now relate the well map to a generalized standard map. The motion of a free particle inside the potential well $V_{sq}(x)$ is related to the motion of a free rotator, the difference being one of boundary conditions. Both free motions are same unless the particle hits the walls. The correspondence between them is made explicit in the following way. Let us consider the dynamics of a free rotator in discrete unit time steps, which is the map relating successive angles θ_n and angular momenta J_n .

$$\theta_{n+1} = \theta_n + J_n \pmod{1} \quad ; \quad J_{n+1} = J_n. \quad (4)$$

Here the motion is confined to a cylinder $[-1/2, 1/2) \times (-\infty, \infty)$. Similarly the discretized free motion in a well of unit width is

$$X_{n+1} = (-1)^{M_n}(X_n + P_n) + (-1)^{M_n+1}\text{Sgn}(P_n)M_n \quad ; \quad P_{n+1} = (-1)^{M_n}P_n \quad (5)$$

Let us denote $S_n \equiv (\theta_n, J_n)$, and $W_n \equiv (X_n, P_n)$. If we have the same initial condition for both the maps (4) and (5) i.e., $W_0 = S_0$, we have the following relation after the n th iterate:

$$W_n = (-1)^M S_n \quad (6)$$

where $M = \sum_{i=0}^{n-1} M_i$, is the *total* number of bounces of the particle after $(n-1)$ iterates. In the rest of the paper we consider the mapping

$$\begin{aligned} J_{n+1} &= J_n + (K/2\pi) \sin(2\pi R\theta_n) \\ \theta_{n+1} &= \theta_n + J_{n+1} \pmod{1}. \end{aligned} \quad (7)$$

It is easy to see that we have the same relation (6) between the well map (2) and the map defined in (7) (more precisely the time reversal of this map).

We refer to the map defined in (7) as the *Generalized Standard Map* (GSM). From the above description it is clear that quantitative dynamical features are same for the well map and the GSM. In attempting to analyze the dynamics of the well map, it is sufficient to understand the dynamics of the GSM. Also the map (7) is easier to handle than the well

map, as it is only a slightly generalized version of the well studied standard map ($R = 1$) [2]. When it is stated that the standard map is a one parameter system the implicit assumption is that there is only one length scale. Here there are naturally *two* length scales whose ratio is the cause of many interesting effects. Both the maps (2) and (7) have reflection symmetry about their origin. Below we discuss various dynamical behaviour of the GSM in more detail. Throughout this paper we consider R to assume positive real values only.

III. DYNAMICAL FEATURES

For the standard map (GSM with $R = 1$), when $K \ll 1$, the dynamics is quasi-regular and the phase space is filled with a large number of KAM tori which are *rotationally invariant circles* [8] extending across the phase plane. These closed loops \mathcal{C} encircle the cylinder and are invariant, meaning that $\mathcal{T}\mathcal{C} = \mathcal{C}$, where \mathcal{T} is an area preserving *continuous* transformation on the cylinder (for instance Eqn.(7) with $R = 1$). KAM tori are the principal barriers for the unstable orbits to diffuse in the phase space. As K increases there is a *smooth* transition from regular to chaotic behaviour with a reduction in the number of KAM tori. Dynamical changes of KAM tori with increase of K are discussed in [9]. At $K \simeq 1$ all the KAM tori disappear from the phase space [10]; the dynamics is chaotic and diffusive for $K \gg 1$. Note that the GSM is periodic in J and θ with unit period. For integer values of R , it is continuous and takes the form of standard map with $K \rightarrow KR$. In this case dynamical transitions are identical with that of the standard map. As the effective perturbation here is KR , higher integer values of R also make the dynamics more chaotic.

When R assumes non-integer values the situation is entirely different from the earlier case, particularly when K is small. Shown in Fig. 1 are typical phase space structures of the GSM for $R \neq 1$ and $0 < R < 2$ at small K . It is seen that no KAM tori exist even when R is slightly away from unity. In general, no KAM tori appear in the phase space when R departs from integer values. This is of course due to the discontinuity in the map when R assumes non-integer values. In other words, there are no closed loops \mathcal{C} encircling the cylinder such that $\mathcal{T}'\mathcal{C} = \mathcal{C}$, where \mathcal{T}' is the transformation defined by GSM with non-integer values of R . As can be seen easily the discontinuity in \mathcal{T}' arises at $\theta = -1/2$ (or $1/2$).

This discontinuous dynamics implies the abrupt breakup of KAM tori and a failure of the Poincaré- Birkhoff scenario. The modifications that may occur are little understood, and Chirikov in [11] points out that the piecewise linear sawtooth map ($p_{n+1} = p_n + K x_n$, $x_{n+1} = x_n + p_{n+1} \bmod 1$) when K is a non-integer such that $-4 < K < 0$ is one such system where extremely complicated locally stable motions occur and “it is not at all clear what could be a meaningful description, if any, of this apparently trivial model”. The particle in a well naturally gives rise to a non-linear generalization of the sawtooth map and below we show how a simple method may give us significant local stability information that explains the dramatic differences observed in Fig. 1.

In addition Fig. 1 distinguishes the dynamics between the cases $R \lesssim 1$ and $R \gtrsim 1$. The former case is more chaotic and the phase space is filled with unstable orbits, while many regular and chaotic regions are seen in the latter. Thus the entire standard map may be regarded as being poised at a point of bifurcation when regarded as a function of the parameter R . However, it is seen that when K is large, there is no such apparent difference

in dynamics between the above two cases since the phase space becomes chaotic and diffusive in both the cases.

A. Stability of the tori

In the absence of the general KAM theorem for irrational tori and the Poincaré-Birkhoff theorem for rational tori, we expect to apply some kind of local analysis to study deviations from integer values of R . Indeed we will see that the integer values of R could be thought of as bifurcation points for entire orbits. We noted earlier that even for small values of K no KAM tori exist in the phase space of the GSM when R departs from unity. To explain the stability changes we look at the behaviour of a single irrational KAM torus, which exists at $R = 1$, as R varies. A typical observation (Fig. 2) shows that KAM torus becomes unstable and chaotic for $R \lesssim 1$ while it is replaced by a chain of stable islands for $R \gtrsim 1$.

We begin by performing a linear stability analysis for a KAM tori with respect to R . We assume below that K is small enough for such an orbit to exist. Let us denote a GSM (with $R = k$, positive integer) KAM orbit as $\{\tilde{\theta}_n, \tilde{J}_n\}$. This satisfies the following mapping:

$$\begin{aligned}\tilde{J}_{n+1} &= \tilde{J}_n + (K/2\pi) \sin(2\pi k \tilde{\theta}_n) \\ \tilde{\theta}_{n+1} &= \tilde{\theta}_n + \tilde{J}_{n+1} \pmod{1}.\end{aligned}\tag{8}$$

Also consider an orbit $\{\theta_n, J_n\}$ of the GSM with $R = k + \mu$ and $|\mu| \ll 1$, with the same initial conditions as the above KAM orbit. Let us introduce the differences $\Delta\theta_n = \theta_n - \tilde{\theta}_n$; $\Delta J_n = J_n - \tilde{J}_n$. Then it is possible to write an exact mapping equation for $\Delta\theta$, ΔJ as

$$\begin{aligned}\Delta J_{n+1} &= \Delta J_n + (K/2\pi) \left\{ \sin\left(2\pi(k + \mu)(\tilde{\theta}_n + \Delta\theta_n)\right) - \sin(2\pi k \tilde{\theta}_n) \right\} \\ \Delta\theta_{n+1} &= \Delta\theta_n + \Delta J_{n+1}.\end{aligned}\tag{9}$$

Expanding in terms of $\Delta\theta_n$ and retaining first order terms leads to a time dependent force and the non-autonomous linear set of equations:

$$\begin{aligned}\Delta J_{n+1} &= \Delta J_n + K(k + \mu) \cos(2\pi(k + \mu)\tilde{\theta}_n) \Delta\theta_n + A_n \\ \Delta\theta_{n+1} &= \Delta\theta_n + \Delta J_{n+1}\end{aligned}\tag{10}$$

with

$$A_n = \frac{K}{2\pi} \left\{ \sin(2\pi(k + \mu)\tilde{\theta}_n) - \sin(2\pi k \tilde{\theta}_n) \right\}.$$

The behaviour of such linear non-autonomous equations can be quite complex (compare for instance the Mathieu differential equation which also arises in linear stability analysis). For our analysis on the stability of the tori we wish be intuitive and derive rough but useful estimates. Although we never expand R about an integer, here we assume that this excursion is small, so that we can treat the non-autonomous stability equations perturbatively. Appealing to the method of averaging we simply replace the time dependent force by its time average. The limitation of this is pointed out further ahead.

Also since the motion on the KAM torus is ergodic in $\tilde{\theta}$, we replace the time average by an equivalent space average with uniform measure. Thus

$$\cos(2\pi R\tilde{\theta}_n) \approx g(R) = \int_{-1/2}^{1/2} \cos(2\pi Rx) dx \quad (11)$$

This procedure leads us to:

$$\begin{aligned} \Delta J_{n+1} &= \Delta J_n + (K/\pi) \sin(\pi(k + \mu)) \Delta\theta_n + A_n \\ \Delta\theta_{n+1} &= \Delta\theta_n + \Delta J_{n+1}. \end{aligned} \quad (12)$$

Eqn.(12) is a simple linear map and its stability can be seen from the corresponding Jacobian matrix which gives the stability condition $|2 + (K/\pi) \sin(\pi(k + \mu))| < 2$. This leads to the following window of stability:

$$-\frac{4\pi}{K} < (-1)^k \sin(\pi\mu) < 0. \quad (13)$$

The above stability window implies that if k is odd KAM tori which exist at $R = k$ are stable for $\mu \gtrsim 0$ and unstable for $\mu \lesssim 0$; converse is the case if k is even. Although μ is small in the above analysis, our numerical observations satisfy the stability condition (13) even for large values of μ (see Fig. 2, which is with $k = 1$). This explains large phase space regions in Fig. 1.

Before dwelling more in this region of phase space we divert attention to those where this procedure has failed. The chaotic regions around $(J = 0, \theta = 0)$ in Fig. 1 for instance presents such a case. In the interior of the original 0/1 resonance (at $R = 1$) even a reversal of the stability criteria is observed. The hyperbolic fixed point at $R = 1$ persists for $R \neq 1$ and is the genesis of the chaos. The smooth stable and unstable manifolds of the hyperbolic fixed point that exist for $R = 1$ and small K cannot exist for $R \neq 1$ as they would then represent rotationally invariant curves. Therefore the presence of the hyperbolic points necessarily implies chaos.

Within the framework of the stability analysis done earlier what has failed around the hyperbolic fixed points is the assumption of uniform measure. If we think of the simple pendulum we are moving from energetic rotational motions (KAM) to slow oscillations of large amplitude and clearly the time is spent preferentially around the turning points. Also the replacement with time averages will fail as the time scales involving fast θ motions and slow ΔJ motions become comparable. The latter effect becomes important as we move into the 0/1 resonance region. We note that the question of the existence of two different time scales is initial value dependent and is present in the standard map as well, *i.e.*, it does not arise as a result of the presence of the additional parameter R .

The modified measure can be approximated well by considering the simple pendulum. We now take $k = 1$ for simplicity and consider only excursions of R from unity. The term $\cos(2\pi R\tilde{\theta}_n)$ in Eq. (10) is replaced with the ergodic average:

$$\cos(2\pi R\tilde{\theta}_n) \approx g(R, \theta_c) = \int_{\theta_c}^{1/2} \frac{\cos(2\pi Rx) dx}{\sqrt{E - \cos(2\pi x)}} / \int_{\theta_c}^{1/2} \frac{dx}{\sqrt{E - \cos(2\pi x)}} \quad (14)$$

Here $-1 \leq E \leq 1$ is the scaled energy and θ_c is the turning point given by $\cos(2\pi\theta_c) = E$. This is shown in Fig. 3 and the point where g crosses zero from above ought to be a point where stability is recovered.

This then explains the uniform chaos around the hyperbolic fixed point for $R \neq 1$. This also explains the stability around the wall ($\theta = 1/2, J = 0$) in all cases. However the interior of the resonance is not accessible to the simple theory. Remarkably Fig. 3 predicts a recovery of stability at $\theta_c \approx 0.15$ which is seen when $R = 0.95$ while stability is recovered at a much higher value of θ_c for $R = 1.05$ and is not seen in Fig. 3. This fact we attribute to the failure of the averaging procedure in analyzing non-autonomous equations and have no other recourse than Eq. (10) itself.

As we have noted, hyperbolic fixed points generate chaos when $R \neq 1$. The lack of chaos in the “meat” of the phase space for $R \gtrsim 1$ where there were KAM tori are therefore regions where there is a total absence of hyperbolic points. The Poincaré-Birkhoff theorem concerning the breakup of rational tori into an equal number of hyperbolic and elliptic periodic points is clearly violated. In fact the modified scenario seems to be the creation of only elliptic fixed points for $R \gtrsim 1$ and only hyperbolic points for $R \lesssim 1$. To illustrate this we have shown in Fig. 4 the fate of points on the lines $J = 1/3$ and $J = (\sqrt{5} - 1)/2$. While in the former case three elliptic islands emerge prominently, in the latter one can see chains of elliptic islands with the clear hierarchy of the number of islands 5, 8, 13, 21, 34... deriving from the Fibonacci sequences generating closer approximations to the golden mean.

These island chains alternate as the ratios approach the golden mean. As a limiting case we may think of a golden mean chain, but we have of course not rigorously proved its existence. There appear to be two types of orbits in the stable regions: those that form an island chain and those that meander in the interstitial spaces between island chains on presumably a fractal set. These would then be examples of strange non-chaotic sets in Hamiltonian mechanics. More investigations into these simple systems seems warranted.

We have thus acquired a rather detailed understanding, using simple methods, of the dramatic stability changes that accompanies the introduction of an additional length scale or discontinuity. We may also speculate that this may prove a good way of controlling or enhancing chaos. While our study has been for Hamiltonian systems dissipative systems may also display such a behaviour.

B. Lyapunov Exponents

The Lyapunov exponents can be calculated using the Jacobian matrix of the GSM, which at n th iterate we denote as \mathbf{M}_n . The stability changes induced by R ought to reflect on the exponent somewhat like a phase transition effect on an order parameter. Shown in Fig. 5 is a typical calculation of the positive Lyapunov exponent Λ_+ for $K = 0.1\pi$. The orbit chosen is a KAM torus for $R = 1$ and we, from our earlier discussion, expect it to be unstable for $R < 1$ and stable for $R > 1$ but not too large. It is seen that $\Lambda_+ \simeq 0$ for $R \gtrsim 1$ in the range shown, which corresponds to the regular motion due to the stable islands formed from the orbit; for $R < 1$, $\Lambda_+ > 0$ which indicates the chaotic behaviour of the orbit. Also the orbit has a maximum value of the Lyapunov exponent at $R \simeq 0.5$, and is hence maximally unstable at this point. We now explore this analytically.

The Jacobian has trace

$$|\text{Tr}(\mathbf{M}_n)| = |2 + KR \cos(2\pi R\theta_n)| \quad (15)$$

and hence $|\text{Tr}(\mathbf{M}_n)| > 2$ for $R < 1/2$ as $|\theta_n| \leq 1/2$. We remind the readers that this range of θ_n is the *entire* configuration space and $\theta_n = \pm 1/2$ represent the wall boundaries. Since the Jacobian is only a function of the angle at a given phase space point (and not also the action), we conclude that the Jacobian has real eigenvalues *throughout* the phase space. In other words, the system is hyperbolic for $R < 1/2$. This implies that there are contracting and expanding real directions or alternatively stable and unstable manifolds throughout phase space. It is worth remarking that very few dynamical models are known exactly to be completely chaotic or hyperbolic. These include the sawtooth maps [12], the baker maps, flows on surfaces of constant negative curvature. The standard map even for large values of the parameter K is not proven to be completely hyperbolic. Thus in this context, we place the fact that GSM has a parameter range for which it is completely hyperbolic for all positive values of the parameter K .

The similarity of the GSM, when $R < 1/2$, with the piecewise linear sawtooth maps is made clear by the following linear approximation. We approximate the force $f(\theta_n) = \sin(2\pi R\theta_n)$ in the GSM by a monotonic linear function $2 \sin(\pi R)\theta_n$. This leads to $|\text{Tr}(\mathbf{M}_n)| \approx |2 + (K/\pi) \sin(\pi R)|$. The Lyapunov exponents in this approximation are given by

$$\Lambda_{\pm} = \ln(r \pm \sqrt{r^2 - 1}) \quad (16)$$

where $r = 1 + (K/2\pi) \sin(\pi R)$. It is clear from Fig. 5 that the approximated exponent fits fairly well. Similar agreement was seen for a wide range of initial conditions and different values of K as well. This shows the validity of the above linear approximation for $f(\theta_n)$ when $R < 1/2$, which enables us to understand the gross behaviour of the Lyapunov exponents in this regime. We note that the usual linear approximation $f(\theta_n) \approx 2\pi R\theta_n$ near the origin was found not to be as good as the above approximation.

Although this study has been essentially that of another area-preserving map, we feel that these novel effects are worth emphasizing, especially since the standard map has been realized in the laboratory in the form of kicked cold sodium atoms, and the transitions to chaos in the quantum regime have been studied as noted above. Implementation of the competing length scales in this experiment could lead to novel observable transport effects. Theoretical studies of the quantum dynamics of this system are currently underway.

REFERENCES

- [1] V.I. Arnold, and A. Avez, Ergodic Problems of Classical Mechanics, WA Benjamin, New York (1968).
- [2] B.V. Chirikov, Phys. Rep. 52 (1979) 263.
- [3] F.M. Izrailev, Phys. Rep. 196 (1990) 299.
- [4] F.L. Moore, J.C. Robinson, C.F. Bharucha, Bala Sundaram and M.G. Raizen, Phys. Rev. Lett. 75 (1995) 4598.
- [5] W.A. Lin and L.E. Reichl, Physica D 19 (1986) 145.
- [6] Bambi Hu, Baowen Li, Jie Liu and Yan Gu, Phys. Rev. Lett. 82 (1999) 4224.
- [7] P.B. Wilkinson, T.M. Fromhold, L. Eaves, F.W. Sheard, N. Miura and T. Takamasu, Nature 380 (1996) 608.
- [8] J.D. Meiss., Rev. Mod. Phys. 64 (1992) 795.
- [9] S.J. Shenker and L.P. Kadanoff, J. Stat. Phys. 27 (4) (1982) 631.
- [10] J.M. Greene, J. Math. Phys. 20 (1979) 1183.
- [11] M.-J. Giannoni, A. Voros, and J. Zinn-Justin (eds.), Chaos and Quantum Physics, Les Houches LII (North-Holland, Amsterdam 1991).
- [12] Q. Chen, I. Dana, J. D. Meiss, and I. C. Percival, Physica D 46 (1990) 217.

Figure Captions

Fig 1 : Phase space of the GSM (with $R \neq 1$) at $K = 0.1\pi$. No KAM tori are seen in any of the cases.

Fig 2 : Shown is an orbit with initial condition $S_0 = (0, 0.34)$, at $K = 0.1\pi$, which corresponds to a KAM torus when $R = 1$. For $R \lesssim 1$, the orbit becomes unstable and chaotic, while for $R \gtrsim 1$ it becomes chain of stable islands.

Fig 3 : The function $g(R, \theta_c)$ which when positive determines the instability of some GSM orbits.

Fig 4 : Orbits with initial conditions on the line $J = 1/3$ (top) and $J = (\sqrt{5}-1)/2$ (bottom) for $K = 0.1$ and $R = 1.05$.

Fig 5 : Positive Lyapunov exponent (dots) of the orbit shown in Fig. 2. The exponent is positive for $R < 1$ with maximum at $R \simeq 0.5$ and zero for $1 < R < 2$. Solid curve is the approximation (16) for $R < 1/2$.

FIGURES

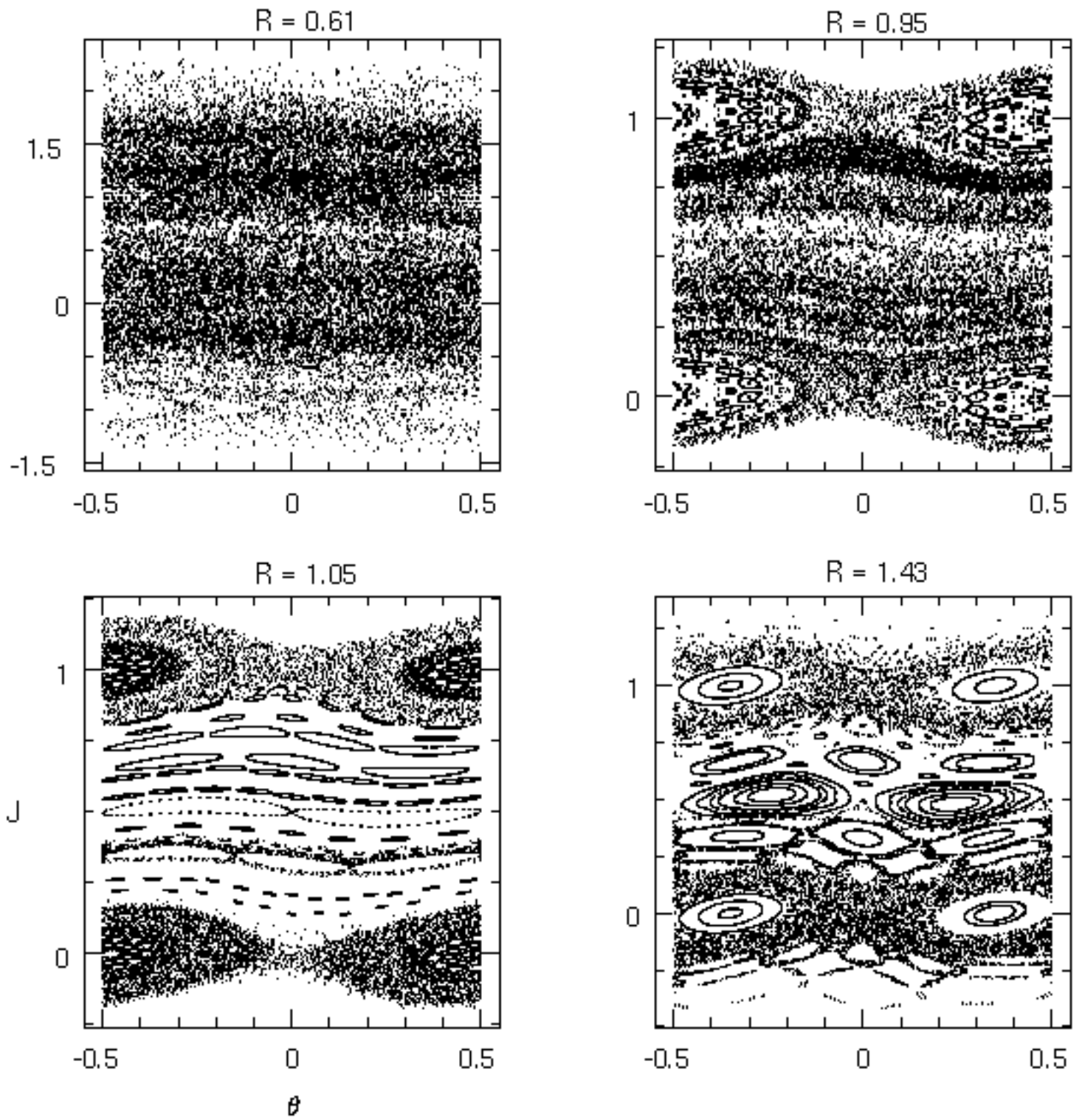


FIG. 1.

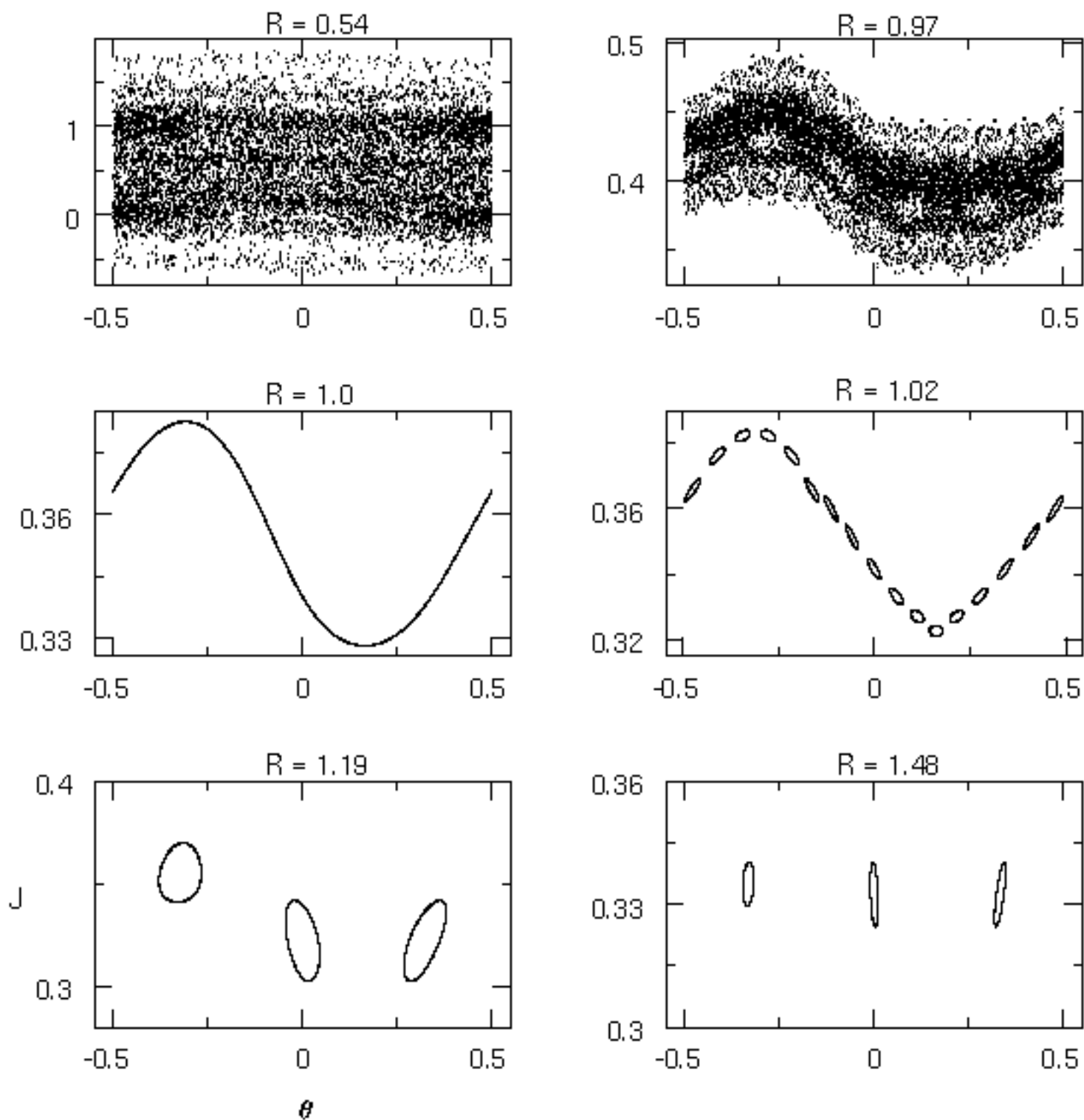


FIG. 2.

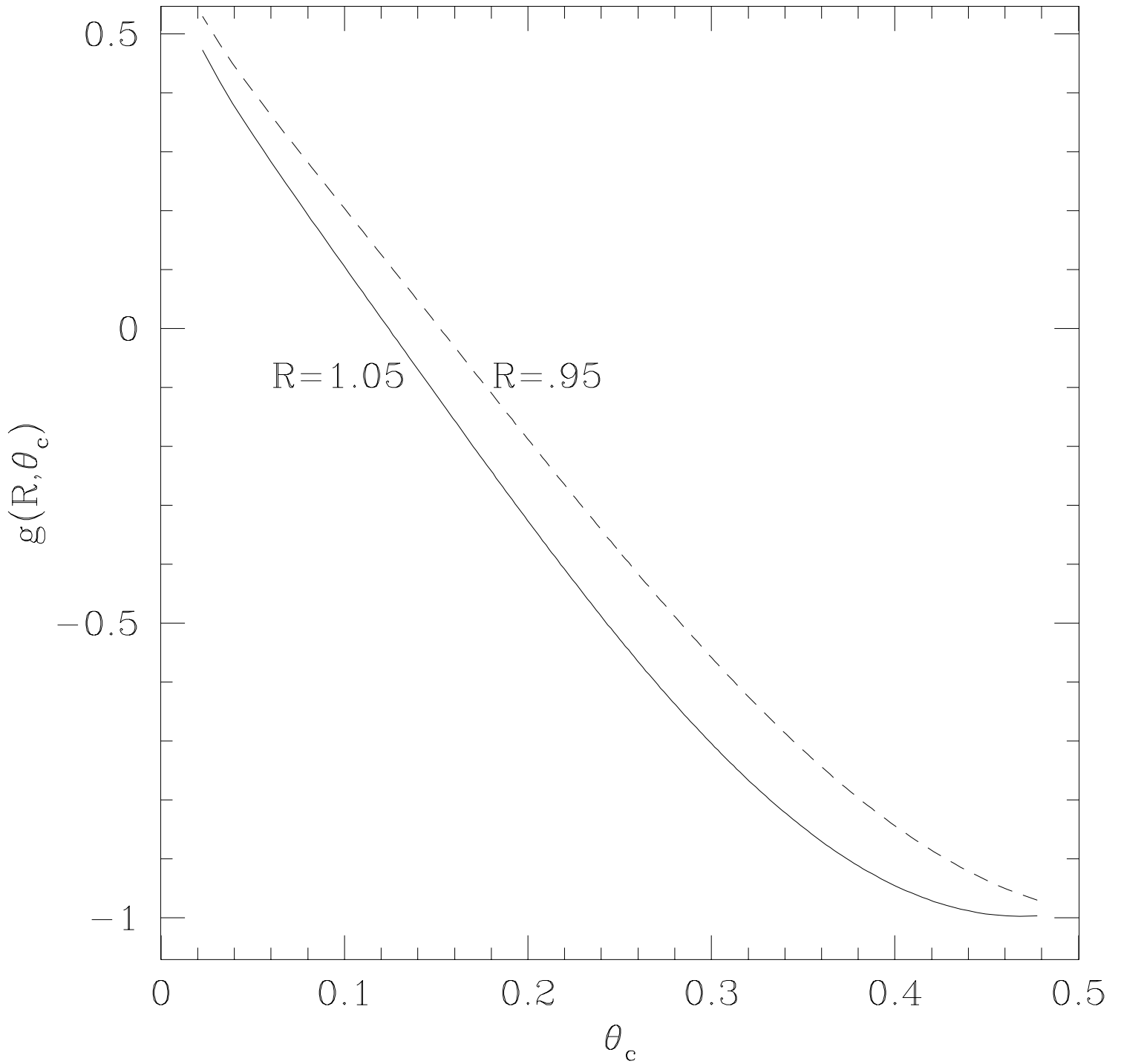


FIG. 3.

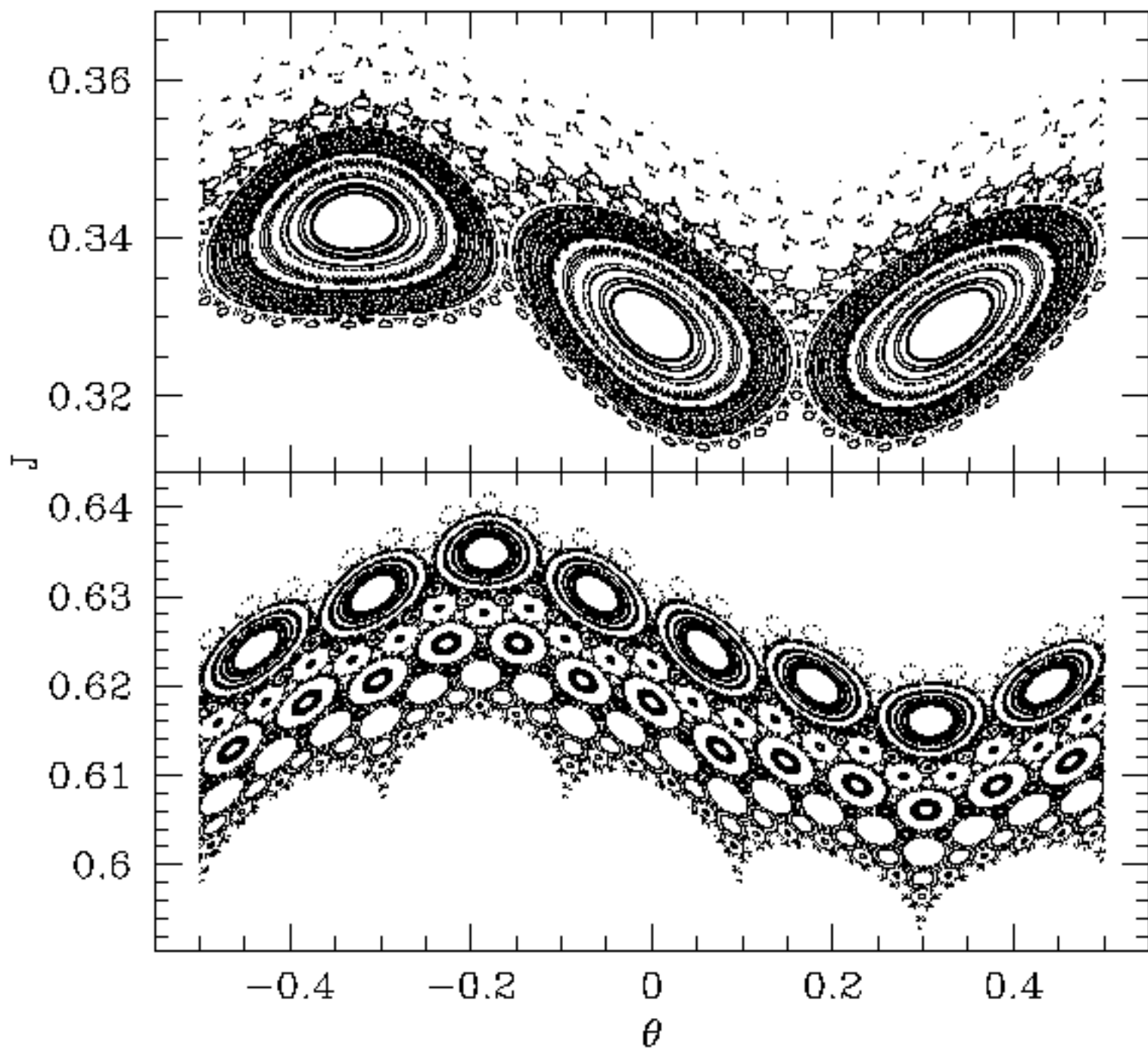


FIG. 4.

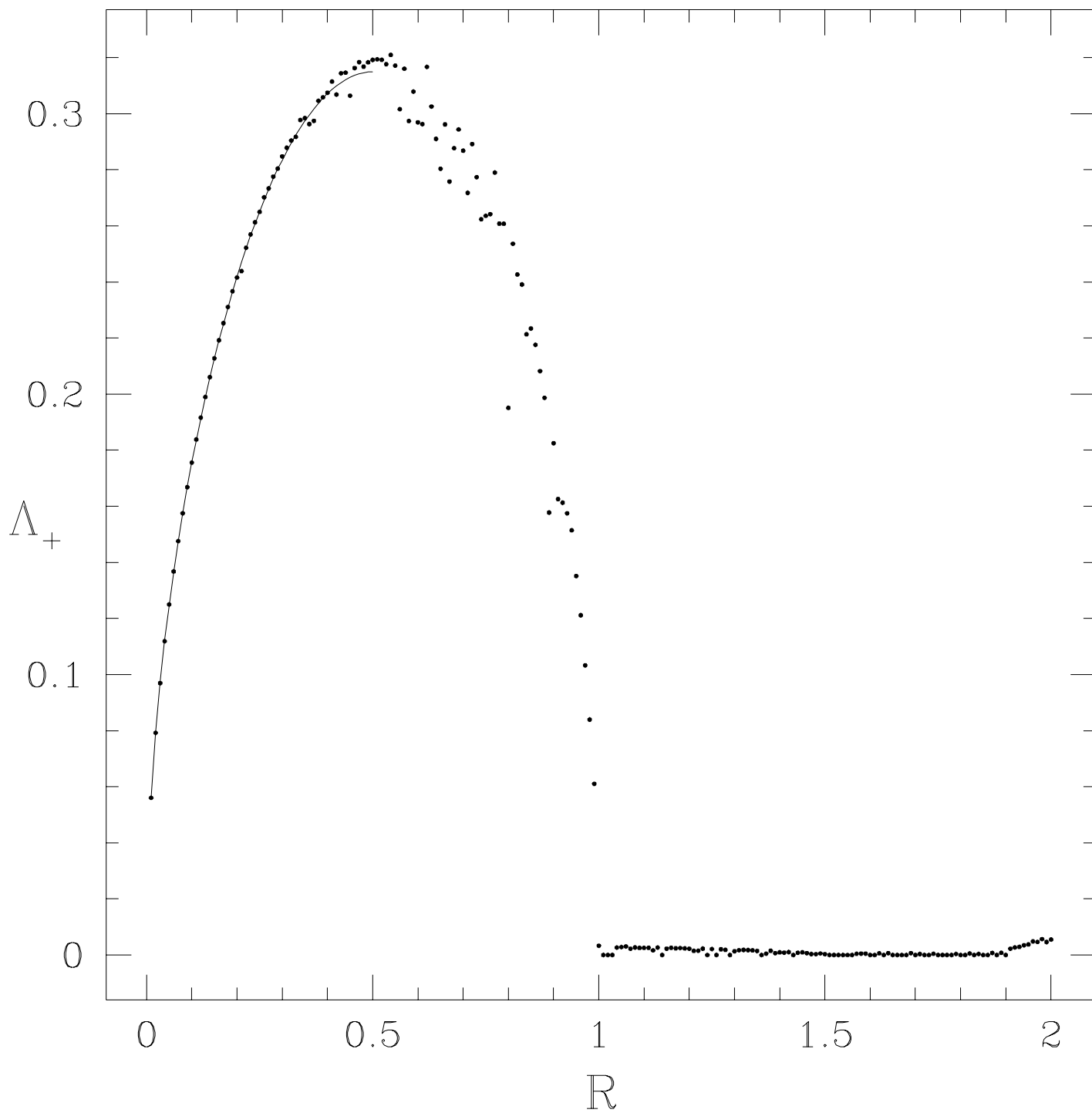


FIG. 5.